Multiqubit noise deconvolution and characterization

Simone Roncallo [*], Lorenzo Maccone [†], and Chiara Macchiavello [‡]

Dipartimento di Fisica, Università degli Studi di Pavia, Via Agostino Bassi 6, 27100 Pavia, Italy
and INFN, Sezione di Pavia, Via Agostino Bassi 6, 27100 Pavia, Italy

We present a noise deconvolution technique for obtaining noiseless expectation values of noisy observables at the output of multiqubit quantum channels. For any number of qubits or in the presence of correlations, our protocol applies to any mathematically invertible noise model, even when its inverse map is not physically implementable, i.e., when it is neither completely positive nor trace preserving. For a generic observable affected by Pauli noise it provides a quadratic speedup, always producing a rescaling of its Pauli basis components. We show that it is still possible to achieve the deconvolution while experimentally estimating the noise parameters, whenever these are unknown (bypassing resource-heavy techniques such as quantum process tomography). We provide a simulation, with examples for both Pauli and non-Pauli channels.
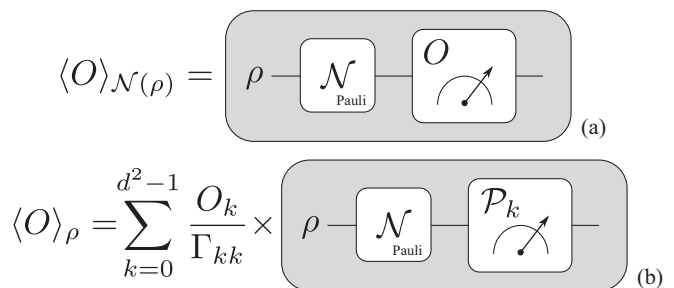
I. INTRODUCTION

Noise in quantum systems can affect the measurement outcome of any observable, modifying the results of measurement-based protocols or procedures, such as state and process tomography [1–4] or quantum simulator experiments [5]. This has also important consequences in quantum computation: Noise sensitivity remains one of the main drawbacks that prevents quantum computers from outperforming their classical counterparts. Several noise mitigation techniques have been considered in the literature, aimed to reduce errors and potential loss of data in the computation process [6–8]. Recently, a noise deconvolution technique was illustrated for observables of single-qubit systems [9], by means of a tomographic reconstruction formula that acts like a postprocessing operation on the noisy data, without introducing modifications to the system.

In this paper we discuss a deconvolution technique that applies to any multiqubit (possibly correlated) noise model [10–14], provided its inverse map exists, even if not physically implementable [15]. We modify the point of view of [9], adopting an operational framework that is more suitable for multiqubit implementations. Unlike other approaches in the literature [6,7], our protocol is passively implemented at the data processing stage: It does not require further experimental (or circuital) configurations, nor active modifications of the original system. For this reason, its range of applicability is not limited to quantum computing: It applies to generic quantum measurements on noisy states, e.g., it can be used to reverse open quantum dynamics [16,17].

Our method works in general, e.g., it does not require Markovian correlations. In the specific but important case of Pauli channels [18], it provides a quadratic speedup over other reconstructions. Given an observable O, we show that its noiseless expectation value can be tomographically reconstructed by performing local measurements on those elements of the Pauli basis for which O takes nonzero components and by rescaling them in terms of the corresponding entries of the Pauli transfer matrix (PTM) of the channel [19–21]. This procedure works for any number of qubits and does not require the complete inversion of the noise map, nor the complete calculation of its PTM. For n-qubit Pauli channels the computational complexity of our procedure, i.e., the number of factors required to complete the deconvolution, scales with the number $r = 1, 2, \ldots, d^2$ of nonzero components of O in the Pauli basis, with $d = 2^n$ the Hilbert space dimension ($r = 1$ represents an observable made by exactly one basis element, while $r = d^2$ represents the worst cases in which O has all nonzero components). This scenario is summarized in Fig. 1. Then we discuss a characterization of the noise map that provides the necessary PTM entries in term of a few measurements on the Pauli basis, without running a full

$$\langle O \rangle_{\mathcal{N}(\rho)} = \boxed{\rho - \underset{\text{Pauli}}{\mathcal{N}} - \overset{O}{\diagup} } \quad \text{(a)}$$

$$\langle O \rangle_{\rho} = \sum_{k=0}^{d^2-1} \frac{O_k}{\Gamma_{kk}} \times \boxed{\rho - \underset{\text{Pauli}}{\mathcal{N}} - \overset{\mathcal{P}_k}{\diagup}} \quad \text{(b)}$$

FIG. 1. (a) Expectation value of a multiqubit observable O, affected by Pauli noise $\mathcal{N}$. (b) The same scheme is applied to the nonzero components of O. Deconvolution is achieved by rescaling the noisy data with the corresponding diagonal entry of the Pauli transfer matrix $\Gamma_{\mathcal{N}}$.

[*]simone.roncallo01@ateneopv.it
[†]lorenzo.maccone@unipv.it
[‡]chiara.macchiavello@unipv.it

process tomography of the system. This represents an efficient alternative whenever the theoretical computation of the PTM is not doable, e.g., when the noise parameters are unknown. Finally, we show that our protocols apply also to non-Pauli channels, with reduced efficiency. In this case, we provide the deconvolution from the complete inversion of the PTM and we show that it scales as d^4 in the worst case. So, in essence, our procedure experiences a quadratic gain (d^2 vs d^4) for Pauli channels.

In Sec. II we review the vectorization of operators and channels. In Sec. III we present noise deconvolution for multiqubit Pauli channels, addressing their characterization whenever the noise parameters are unknown. Then we generalize our discussion to the non-Pauli case. In Sec. IV we consider the explicit deconvolution of n-qubit bit-flip and depolarizing correlated noises, simulating the latter for $n = 3$. As a non-Pauli example, we consider a two-qubit amplitude damping correlated channel, which models qubits losses inside devices.

II. VECTORIZATION

We consider the Hilbert space of an n-qubit system. The basis for the set of operators is

$$\left\{ \sigma_{\alpha_1} \otimes \sigma_{\alpha_2} \otimes \cdots \otimes \sigma_{\alpha_n} \middle| \alpha_1, \alpha_2, \ldots, \alpha_n = 0, 1, 2, 3 \right\}, \quad (1)$$

with $\sigma_0 = \mathbb{1}_2$, $\sigma_1 = \sigma_x$, $\sigma_2 = \sigma_y$, and $\sigma_3 = \sigma_z$. We write the Pauli basis in the notation

$$\{ \mathcal{P}_k \mid k = 0, 1, 2, 3, \ldots, d^2 - 1 \}, \quad (2)$$

with $d = 2^n$ and $\mathcal{P}_k$ denoting the generic element of Eq. (1) in lexicographic order. We introduce the vectorized representation [19], in which each element of the basis $\mathcal{P}_k$ is mapped to a vector $|k\rangle\rangle$. In this space, an operator A is represented as a $1 \times d^2$ column vector

$$|A\rangle\rangle = \sum_{k=0}^{d^2-1} A_k |k\rangle\rangle, \quad (3)$$

with $A_k = \langle\langle k|A\rangle\rangle$ given by the Hilbert-Schmidt inner product

$$\langle\langle A|B\rangle\rangle := \frac{1}{d}\mathrm{Tr}[A^\dagger B], \quad (4)$$

with B any operator on this Hilbert space.

Consider a quantum system in the state ρ. A quantum channel is a linear completely positive and trace-preserving (CPTP) map that modifies the system state as $\rho \to \Phi(\rho)$. In the vectorized framework, a channel Φ is represented by a $d^2 \times d^2$ matrix

$$\Gamma_\Phi = \sum_{j,q=0}^{d^2-1} \Gamma_{jq} |j\rangle\rangle\langle\langle q|, \quad (5)$$

with components given by the Hilbert-Schmidt inner product

$$\Gamma_{jq} = \langle\langle j|\Gamma_\Phi|q\rangle\rangle = \frac{1}{d}\mathrm{Tr}[\mathcal{P}_j \Phi(\mathcal{P}_q)]. \quad (6)$$

This is called the Pauli transfer matrix of the channel [19]. In this representation, the action of the channel $\Phi(A)$ is given by

a matrix-vector multiplication

$$|\Phi(A)\rangle\rangle = \Gamma_\Phi |A\rangle\rangle = \sum_{j,q=0}^{d^2-1} \Gamma_{jq} A_q |j\rangle\rangle. \quad (7)$$

The CPTP condition guarantees that $\Gamma_{0q} = \delta_{0q}$, with δ_{jq} the Kronecker delta. For unital channels, i.e., when $\Phi(\mathbb{1}) = \mathbb{1}$, it holds also that $\Gamma_{j0} = \delta_{j0}$.

Consider a channel Φ, its adjoint Φ^* is the map satisfying

$$\langle\langle A|\Phi^*(B)\rangle\rangle = \langle\langle \Phi(A)|B\rangle\rangle. \quad (8)$$

This implies that the adjoint PTM, here denoted by Γ_Φ^*, is precisely the Hermitian conjugate of Γ_Φ.

III. NOISE DECONVOLUTION

Noise in open quantum systems is modeled in terms of quantum channels [1], namely, linear CPTP operations $\mathcal{N}$ that map the ideal, i.e., noiseless, state ρ into a noisy one $\rho' = \mathcal{N}(\rho)$. Different choices of $\mathcal{N}$ correspond to different noise models, e.g., the bit-flip, the dephasing, the depolarizing, or the amplitude damping noises [1]. With the state modified by $\mathcal{N}$, any measurement performed on an observable O becomes noisy, namely, its expectation value $\langle O\rangle_\rho$ is mapped to $\langle O\rangle_{\rho'}$. In this section we introduce noise deconvolution as a technique that provides the ideal expectation value $\langle O\rangle_\rho$ of arbitrary operators, using the noisy data obtained on ρ'. Our protocol applies to any mathematically invertible noise model, i.e., one for which $\Gamma_\mathcal{N}^{-1}$ exists, even when the inverse channel is not physically implementable, i.e., when $\mathcal{N}^{-1}$ is not CPTP.

We consider the noise deconvolution equation derived in [9],

$$\langle O\rangle_\rho = \langle \mathcal{N}^{*^{-1}}(O)\rangle_{\rho'}, \quad (9)$$

which yields the ideal (i.e., noiseless) expectation value of an arbitrary observable $\langle O\rangle_\rho$ (or even of a non-observable operator) by evaluating instead the inverted adjoint map $\mathcal{N}^{*^{-1}}(O)$ over the noisy state $\rho' = \mathcal{N}(\rho)$. In other proposals [22], similar inversions are implemented physically (often only approximately) by introducing suitable modifications to the channel. Here instead we just use the noisy measured data to calculate the noiseless value. In other words and in contrast to previous proposals, our noise-inversion reconstruction is implemented entirely and solely at the data processing stage. In the vectorized framework, Eq. (9) reads

$$\langle\langle \rho|O\rangle\rangle = \langle\langle \rho'|\Gamma_\mathcal{N}^{*^{-1}}|O\rangle\rangle, \quad (10)$$

where $\Gamma_\mathcal{N}^{*^{-1}}$ is the inverse adjoint PTM.

We start with the deconvolution of multiqubit Pauli channels, for which the vectorization guarantees a quadratic speedup in efficiency over the general case (treated below). The current method generalizes and supersedes the single-qubit analysis presented in [9]. In this case we derive a reconstruction formula without completely inverting the noise channel, instead using only some components of the PTM. We first apply this procedure to an observable made by one of the possible n-fold tensor products of the Pauli matrices, i.e. one of the elements of the basis; then we extend our considerations to the expectation value of a generic observable that takes

all the contributions from the Pauli basis. At the end of the section, we generalize our discussion to the non-Pauli case.

In the Pauli basis, the Kraus representation [1] of an n-qubit Pauli channel is [18]

$$\mathcal{N}(\rho) = \sum_{j=0}^{d^2-1} \beta_j \mathcal{P}_j \rho \mathcal{P}_j, \qquad (11)$$

with $\sum_j \beta_j = 1$ and $\beta_j \geqslant 0 \, \forall \, j$. Such channels represent an example of random unitary maps [23], where each unitary $\mathcal{P}_j$ is applied with probability β_j. In the case of Eq. (11), this produces a depolarizing contraction of the Bloch hypersphere, whose intensity and direction depend on the choice of β_j [24].

A Pauli channel yields a diagonal PTM

$$\Gamma_{\mathcal{N}} = \sum_{j=0}^{d^2-1} \lambda_j |j\rangle\!\rangle\langle\!\langle j|, \qquad (12)$$

where $\lambda_j = \langle\!\langle j|\Gamma_{\mathcal{N}}|j\rangle\!\rangle$. As the only requirement, we ask $\Gamma_{\mathcal{N}}$ to be mathematically invertible, i.e., that $\lambda_j \neq 0 \, \forall \, j$.[1] For now, we also assume that the noise parameters are known so that a theoretical computation of the PTM is always possible. This last assumption simplifies our analysis, but it is not necessary. We discuss the case of unknown noise in the following paragraphs.

Since all the Kraus operators in Eq. (11) are Hermitian, the adjoint of the Pauli channel is the channel itself [9], yielding $\Gamma_{\mathcal{N}}^{*^{-1}} = \Gamma_{\mathcal{N}}^{-1}$. Then the inverse PTM is diagonal too and its components read $1/\lambda_j$.

First, consider an observable given by the kth element of the basis, which in vectorized notation corresponds to a column vector with only one nonzero component $|O\rangle\!\rangle = |k\rangle\!\rangle$. The action of the inverse PTM yields

$$\Gamma_{\mathcal{N}}^{-1}|O\rangle\!\rangle = \Gamma_{kk}^{-1}|k\rangle\!\rangle = \frac{1}{\lambda_k}|k\rangle\!\rangle. \qquad (13)$$

Using Eq. (10), the expectation value follows as $\langle\!\langle \rho|k\rangle\!\rangle = \lambda_k^{-1}\langle\!\langle \rho'|k\rangle\!\rangle$, which in standard nonvectorized notation reads

$$\langle\mathcal{P}_k\rangle_\rho = \frac{d}{\text{Tr}[\mathcal{P}_k\mathcal{N}(\mathcal{P}_k)]}\langle\mathcal{P}_k\rangle_{\rho'}. \qquad (14)$$

This shows that for an n-qubit Pauli channel, the deconvolution of the expectation value of the kth element of the basis is always obtained as a rescaling of the noisy outcome, which depends on the kth element on the diagonal of the inverse PTM.

We now discuss the deconvolution of a generic observable O subject to an arbitrary n-qubit Pauli channel. We expand O in terms of the basis vectors $|O\rangle\!\rangle = \sum_k O_k |k\rangle\!\rangle$ to compute the right-hand side of Eq. (10). Applying the same strategy, each component O_k must be rescaled by the corresponding element on the diagonal of the inverse PTM. Then the reconstructed

measurement outcome reads

$$\langle O\rangle_\rho = \sum_{k=0}^{d^2-1} \frac{d}{\text{Tr}[\mathcal{P}_k\mathcal{N}(\mathcal{P}_k)]} O_k \langle\mathcal{P}_k\rangle_{\rho'}. \qquad (15)$$

Namely, we obtain the ideal noiseless outcome, i.e., over ρ, by processing the noisy expectation values, i.e., over $\rho' = \mathcal{N}(\rho)$, of those Pauli basis elements $\mathcal{P}_k$ that contribute to the expansion of O.

This procedure works for any number n of (even correlated) qubits and it involves only local measurements on each element of the basis. The computational complexity, i.e., the number of factors required, scales with the number $r = 1, 2, \ldots, d^2$ of nonzero elements of the expansion of O on the Pauli basis. In the trivial case in which O is exactly an n-qubit Pauli matrix, the deconvolution always requires a single measurement and one PTM entry, for any number of qubits. On the other hand, when O is a generic observable, the deconvolution requires a measurement on the entire basis and the computation of all the d^2 diagonal components of the PTM. In any case, this considerably reduces the number of computations of the PTM entries over the inversion-based method of [9], which for n qubits always requires d^4 operations.

So far we have considered n-qubit Pauli channels whose parameters are known *a priori*. Although it simplifies the analysis, this assumption is not necessary: We can still estimate these parameters without running a full process tomography of the channel [1,3], which is intractable for large n. For a general n-qubit Pauli channel $\mathcal{N}$, with unknown Kraus representation coefficients in Eq. (11), the deconvolution is achieved by means of the following characterization. Prepare the system in the state

$$\rho_k = \frac{\mathbb{1} + \mathcal{P}_k}{d} \quad \text{for } k \neq 0, \qquad (16)$$

with $\mathbb{1}$ the n-qubit identity operator (see the Appendix for a discussion on positivity). Assuming that ρ_k evolves to $\rho_k' = \mathcal{N}(\rho_k)$, i.e., that the channel acts independently of the preparation scheme of Eq. (16), unitality guarantees that

$$\rho_k' = \frac{\mathbb{1} + \mathcal{N}(\mathcal{P}_k)}{d}. \qquad (17)$$

The diagonal entries of the PTM then read

$$\Gamma_{kk} = \langle\mathcal{P}_k\rangle_{\rho_k'} \quad \text{for } k \neq 0, \qquad (18)$$

with $\langle\mathcal{P}_k\rangle_{\rho_k'} = \text{Tr}[\mathcal{P}_k\mathcal{N}(\rho_k)]$, which can be used in the deconvolution formula (14) or (15). This means that, even without knowing the noise parameters, we can still obtain the reconstruction factors by measuring the kth element of the Pauli basis over a noisy state initially prepared as in Eq. (16). Again, this requires at most r operations, with $r = 1, 2, \ldots, d^2$ the number of nonzero components of O in the Pauli basis. We

_____

[1]An example of a noninvertible map is represented by a depolarizing channel with $p = 1$, for which the Bloch hypersphere collapses to a single point.

summarize the entire procedure in Protocol 1.

Protocol 1 Multiqubit Pauli channel deconvolution.

Input: Observable O **Optional:** Pauli channel $\mathcal{N}$
Result: Noiseless expectation value $\langle O \rangle_\rho$
1: construction of the basis $\triangleright$ $\{\mathcal{P}_k\}$ for $k = 0, 1, \ldots, d^2 - 1$
2: projection of O on the basis $\qquad \triangleright$ $O_k = \text{Tr}[O\mathcal{P}_k]/d$
3: **for** k such that $O_k \neq 0$ **do**
4: $\quad$ noisy measurement on the basis $\qquad \triangleright$ $\langle \mathcal{P}_k \rangle_{\mathcal{N}(\rho)}$
5: $\quad$ **if** $\mathcal{N}$ is known **then**
6: $\qquad$ get PTM $\qquad \triangleright$ $\Gamma_{kk} \leftarrow \text{Tr}[\mathcal{P}_k \mathcal{N}(\mathcal{P}_k)]/d$
7: $\quad$ **else**
8: $\qquad$ state preparation $\qquad \triangleright$ $\rho_k = (\mathbb{1} + \mathcal{P}_k)/d$
9: $\qquad$ PTM characterization $\qquad \triangleright$ $\Gamma_{kk} \leftarrow \langle \mathcal{P}_k \rangle_{\mathcal{N}(\rho_k)}$
10: noise deconvolution $\qquad \triangleright$ $\langle O \rangle_\rho \leftarrow \sum_k \Gamma_{kk}^{-1} O_k \langle \mathcal{P}_k \rangle_{\mathcal{N}(\rho)}$

Before considering the applications, we discuss the case of noise channels that cannot be expressed in the form of Eq. (11), i.e., whose Kraus representation contains at least one operator that is different from a Pauli $\mathcal{P}_k$. These channels describe purely quantum mechanical processes, e.g., a "spontaneous emission", which is modeled by the amplitude damping channel [1].

Non-Pauli channels are not self-adjoint and have a nondiagonal PTM, so $\Gamma_{\mathcal{N}}^{*^{-1}}$ cannot be simply obtained as in Eq. (13). In this case, the tomographic reconstruction formula of a generic observable O reads

$$\langle O \rangle_\rho = \sum_{j,q=0}^{d^2-1} (\Gamma^{*^{-1}})_{jq} O_q \langle \mathcal{P}_j \rangle_{\rho'}, \tag{19}$$

which, in the case of $O = \mathcal{P}_k$, i.e., $O = |k\rangle\rangle$ in the vectorized notation, reduces to

$$\langle \mathcal{P}_k \rangle_\rho = \sum_{j=0}^{d^2-1} (\Gamma^{*^{-1}})_{jk} \langle \mathcal{P}_j \rangle_{\rho'}. \tag{20}$$

In this case, the deconvolution procedure still works, although less efficiently: It requires more computations and the complete calculation of the inverse adjoint PTM $\Gamma_{\mathcal{N}}^{*^{-1}}$. For Pauli channels, both equations consistently reduce to Eqs. (14) and (15). In the next section we consider the explicit deconvolution of a two-qubit amplitude damping correlated channel.

When noise is not described by a Pauli channel, as it often occurs in real devices, the quadratic speedup of Eq. (15) is not achievable. However, generic noise models are usually split in terms of Pauli and non-Pauli (but simpler) contributions. See, for example, [9], where the decoherence of Rigetti Aspen-9 is modeled as a composition of a dephasing (Pauli) and an amplitude damping (non-Pauli) channel. In the vectorized representation, the composition of multiple channels reduces to the product of their PTM. Even in this case, their deconvolution can be separately treated, with still a quadratic advantage on the Pauli terms, which then act as a rescaling of the non-Pauli rows or columns. Alternatively, twirling techniques can be employed to remove the off-diagonal elements of the PTM [18,25], thus mapping the original channel to an effective Pauli one.

Similarly to the diagonal case, a straightforward characterization can be employed whenever the channel is unital and its parameters are unknown. Prepare the system in the state ρ_k of Eq. (16) evolved to Eq. (17) and then iterate Eq. (18) for all the elements $\mathcal{P}_j$ of the Pauli basis, yielding the PTM as

$$\Gamma_{jk} = \langle \mathcal{P}_j \rangle_{\rho'_k} \quad \text{for } j, k \neq 0, \tag{21}$$

which can be inverted and substituted in Eq. (19) or (20).

Both Eqs. (18) and (21) provide a direct tomographic reconstruction of the channel PTM, as long as the channel is unital. This represents an alternative to the standard approach that recovers the channel Kraus representation through standard quantum process tomography (a generalization of this procedure to nonunital channels and a comparison with quantum process tomography will be discussed in [26]).

IV. APPLICATIONS

In this section we discuss noise deconvolution of several examples of Pauli and non-Pauli noise models. To analyze correlations we demonstrate our general method on a specific class of channels, in which a parameter μ measures the amount of correlations [10–12,27,28].

We start with the class of Pauli correlated channels defined in [10–12], whose Kraus representation reads

$$\mathcal{N}(\rho) = \sum_{\{\alpha_i\}=0}^{3} p_{\alpha_1\alpha_2\cdots\alpha_n} A_{\alpha_1\alpha_2\cdots\alpha_n} \rho A^\dagger_{\alpha_1\alpha_2\cdots\alpha_n}, \tag{22}$$

with $i \in \{1, 2, \ldots, n\}$ and Kraus operators

$$A_{\alpha_1\alpha_2\cdots\alpha_n} = \sigma_{\alpha_1} \otimes \sigma_{\alpha_2} \otimes \cdots \otimes \sigma_{\alpha_n}, \tag{23}$$

with $p_{\alpha_1\alpha_2\cdots\alpha_n} = p_{\alpha_1} p_{\alpha_2|\alpha_1} \cdots p_{\alpha_n|\alpha_{n-1}}$ given by the Markov chain [12,29]

$$p_{\alpha_j|\alpha_i} = (1 - \mu) p_{\alpha_j} + \mu \delta_{\alpha_i \alpha_j}, \tag{24}$$

$$\vec{p} = [1 - p, p_x, p_y, p_z]^T, \tag{25}$$

with $p = p_x + p_y + p_z$. This kind of correlation is not a requirement of our deconvolution technique; it provides only an example to test our protocol. The parameter $\mu \in [0, 1]$ represents the degree of correlation between couple of qubits. On the one hand, $\mu = 0$ represents a memoryless channel, which is when the qubits are completely uncorrelated. On the other hand, $\mu = 1$ describes a full-memory channel, i.e., when the qubits are completely correlated. The Pauli channels generalize noise models such as the bit-flip, the bit-phase-flip, the dephasing, and the depolarizing which can be reobtained from Eq. (22) by a proper choice of $\vec{p}$. For example, we obtain the bit-flip channel when $\vec{p} = [1 - p, p, 0, 0]^T$ or the depolarizing channel when $\vec{p} = [1 - p, p/3, p/3, p/3]^T$.

As the first example, consider the n-qubit observable $\sigma_z^{\otimes n}$, whose expectation value is affected by a bit-flip correlated noise [1,12], i.e., with $\vec{p} = [1 - p, p, 0, 0]^T$. In this case, the
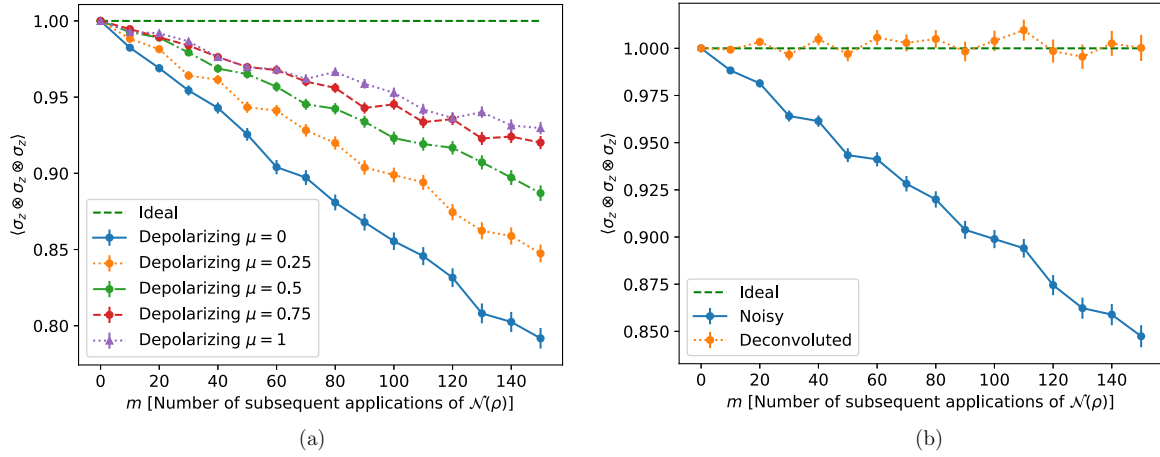
FIG. 2. (a) Simulated noise effect on $\langle \sigma_z^{\otimes 3} \rangle$ for a three-qubit depolarizing correlated channel, where the degree of correlation is parametrized by $\mu \in [0, 1]$ and with probability $q = 0.00052$. The system is initially prepared in the noiseless state $\rho = |000\rangle\langle 000|$. The ideal expectation value $\langle \sigma_z^{\otimes 3} \rangle_\rho = 1$ is represented by a dashed horizontal line. The simulation is performed using QISKIT AER for 8192 shots, with respect to the number m of subsequent applications of the noise map $\mathcal{N}^m(\rho)$. The noise effect is plotted for different values of μ. Note that when the value of μ decreases, the correlation of qubits increases and the effect of the noise decreases. (b) Simulated deconvolution of the noise channel for $\mu = 0.25$. We compare the noisy output with the noiseless one, recovered with the noise deconvolution procedure presented here.

deconvolution formula yields

$$\left\langle \sigma_z^{\otimes n} \right\rangle_\rho = f_n(p, \mu) \left\langle \sigma_z^{\otimes n} \right\rangle_{\rho'}, \qquad (26)$$

where the reconstruction factor is given by

$$f_n(p, \mu) = \frac{2^n}{\text{Tr}\left[\sigma_z^{\otimes n} \mathcal{N}\left(\sigma_z^{\otimes n} \right) \right]}. \qquad (27)$$

By direct computation, we obtain

$$f_1(p, \mu) = \frac{1}{1 - 2p}, \qquad (28)$$

$$f_2(p, \mu) = \frac{1}{1 + 4(\mu - 1)(1 - p)p}, \qquad (29)$$

$$f_3(p, \mu) = \frac{1}{(1 - 2p)[1 + 4(\mu - 1)^2(p - 1)p]}. \qquad (30)$$

For a depolarizing correlated channel [10,12], i.e., when $\vec{p} = [1 - 3q/4, q/4, q/4, q/4]^T$, the same computation gives

$$f_1(q, \mu) = \frac{1}{1 - q}, \qquad (31)$$

$$f_2(q, \mu) = \frac{1}{1 + (\mu - 1)(2 - q)q}, \qquad (32)$$

$$f_3(q, \mu) = \frac{1}{(1 - q)[1 + (\mu - 1)^2(q - 2)q]}. \qquad (33)$$

When the qubits are completely uncorrelated ($\mu = 0$), the noise deconvolution factorizes in terms of the single-qubit contributions. For qubits that are completely correlated ($\mu = 1$), the noise has no effect when n is even, while it is corrected by a single-qubit contribution when n is odd. In Fig. 2(a) we plot the effect of a three-qubit depolarizing correlated channel on $\langle \sigma_z^{\otimes 3} \rangle$ with respect to the number of subsequent applications of the noise map, parametrized in terms of μ. In Fig. 2(b) we perform a simulation of the deconvolution, which successfully reproduces the noiseless expectation value.

As a non-Pauli example, we consider a two-qubit amplitude damping correlated channel [27,28]. For a single-qubit system, the amplitude damping channel is defined in terms of two Kraus operators

$$E_0 = \begin{pmatrix} 1 & 0 \\ 0 & \sqrt{\eta} \end{pmatrix}, \quad E_1 = \begin{pmatrix} 0 & \sqrt{1 - \eta} \\ 0 & 0 \end{pmatrix}, \qquad (34)$$

where $1 - \eta$ represents the probability of the system losing a qubit, e.g., by emitting a photon [1], and it plays the role of channel transmissivity, e.g., in the case of optical fibers [28].

The two-qubit amplitude damping correlated channel can be obtained as a convex combination of a memoryless amplitude damping channel $\mathcal{N}_0$ with a memoryful one $\mathcal{N}_1$,

$$\mathcal{N}(\rho) = (1 - \mu)\mathcal{N}_0(\rho) + \mu \mathcal{N}_1(\rho), \qquad (35)$$

where

$$\mathcal{N}_0(\rho) = \sum_{j=0}^{3} A_j \rho A_j^\dagger, \quad \mathcal{N}_1(\rho) = \sum_{j=0}^{1} B_j \rho B_j^\dagger, \qquad (36)$$

with Kraus operators $A_0 = E_0 \otimes E_0$, $A_1 = E_0 \otimes E_1$, $A_2 = E_1 \otimes E_0$, $A_3 = E_1 \otimes E_1$, and

$$B_0 = \begin{pmatrix} 1 & 0 & 0 & 0 \\ 0 & 1 & 0 & 0 \\ 0 & 0 & 1 & 0 \\ 0 & 0 & 0 & \sqrt{\eta} \end{pmatrix},$$

$$B_1 = \begin{pmatrix} 0 & 0 & 0 & \sqrt{1 - \eta} \\ 0 & 0 & 0 & 0 \\ 0 & 0 & 0 & 0 \\ 0 & 0 & 0 & 0 \end{pmatrix}. \qquad (37)$$

Consider the two-qubit observables $\sigma_x^{\otimes 2}$, $\sigma_y^{\otimes 2}$, and $\sigma_z^{\otimes 2}$ with noisy state $\rho' = \mathcal{N}(\rho)$. From the deconvolution formula and the computation of the inverse adjoint PTM it follows

that

$$\langle \sigma_x^{\otimes 2} \rangle_\rho = f(\eta, \mu) \{ [2\eta(1-\mu) + \mu(\sqrt{\eta} + 1)] \langle \sigma_x^{\otimes 2} \rangle_{\rho'} \\ + \mu(\sqrt{\eta} - 1) \langle \sigma_y^{\otimes 2} \rangle_{\rho'} \}, \tag{38}$$

while $\langle \sigma_y^{\otimes 2} \rangle_\rho$ is obtained from Eq. (38) through the index exchange $x \leftrightarrow y$, and that

$$\langle \sigma_z^{\otimes 2} \rangle_\rho = g(\eta, \mu) [(\mu - 1)^2 (\eta - 1)^2 + \langle \sigma_z^{\otimes 2} \rangle_{\rho'} \\ - (\mu - 1)(\eta - 1) \langle \mathbb{1} \otimes \sigma_z + \sigma_z \otimes \mathbb{1} \rangle_{\rho'}], \tag{39}$$

with

$$f(\eta, \mu) = \frac{1}{2[\mu(\eta - \sqrt{\eta}) - \eta][\mu(\eta - 1) - \eta]}, \tag{40}$$

$$g(\eta, \mu) = \frac{1}{[\eta + \mu(1 - \eta)]^2}. \tag{41}$$

Note that when the qubits are completely uncorrelated ($\mu = 0$) the noise deconvolution factorizes in terms of the single-qubit contributions.[2] When the two qubits are completely correlated ($\mu = 1$) the noise has no effect on $\langle \sigma_z^{\otimes 2} \rangle$.

V. CONCLUSION

We illustrated a procedure for the deconvolution of multi-qubit noise described by mathematically invertible quantum channels: It returns the ideal expectation value of arbitrary observables from the noisy data.

In the case of Pauli channels, our prescription bypasses the inversion of the noise map, providing the deconvolution from a set of Pauli measurements rescaled by a few components of the PTM (where the number of factors is quadratically reduced with respect to the general scenario). As discussed and shown in the simulation, this analysis can be applied to any example of multiqubit Pauli noise, e.g., the bit-flip or the depolarizing correlated channels. Then we presented a characterization technique that provides the necessary PTM entries as a set of Pauli measurements on a specific class of input states, guaranteeing the deconvolution whenever a theoretical approach is not possible, e.g., when the parameters of the channel are unknown.

Finally, we discussed the deconvolution of noise that does not belong to the class of multiqubit Pauli channels. Our procedure successfully applies also to these cases, while less efficiently and requiring the complete computation (and inversion) of the adjoint PTM.

ACKNOWLEDGMENTS

APPENDIX: POSITIVITY OF THE CHARACTERIZATION STATE

In this Appendix we show that the operator used in the noise characterization procedure fulfills all the requirements of a density operator, i.e., Hermiticity, unit trace, and positive semidefiniteness [1], namely, that it represents a state of the n-qubit system.

Consider the operators of Eq. (16), with $k = 1, 2, \ldots, d^2 - 1$. While Hermiticity is straightforward, unit trace follows from $\mathrm{Tr}[\mathcal{P}_k] = 0$ for $k \neq 0$.

To prove positive semidefiniteness, we refer to the characterization of density operators in terms of the coherence vector representation discussed in [30]. Let S_m be the coefficients of the characteristic polynomial of the $d \times d$ matrix representation of ρ,[3] given by

$$S_m = \frac{1}{m} \sum_{j=1}^{m} (-1)^{j-1} \mathrm{Tr}[\rho^j] S_{m-j}, \tag{A1}$$

with $S_0 = 1$ and $m = 0, 1, \ldots, d$.[4]

A necessary and sufficient condition for ρ being positive semidefinite is that $S_m \geqslant 0 \, \forall m$.

Theorem 1. The operator $\rho = (1 + \mathcal{P}_k)/d$ is positive semidefinite.

Proof. Consider the operator $A = (1 + \mathcal{P}_k)/2$, which is positive semidefinite if and only if ρ does. A direct computation yields $A^j = A$ and $\mathrm{Tr}[A^j] = d/2$. For A, Eq. (A1) reads

$$S_m = \frac{d}{2m} \sum_{j=1}^{m} (-1)^{j-1} S_{m-j}. \tag{A2}$$

Extracting the first term of the series and collecting a minus sign, we get

$$S_m = \frac{d}{2m} \left(S_{m-1} - \sum_{j=2}^{m} (-1)^{j-2} S_{m-j} \right). \tag{A3}$$

Translating $j \to j + 1$ (with the sum now running from 1 to $m - 1$) and writing Eq. (A2) for S_{m-1}, we obtain a recursive

---

[3]In this Appendix we use the standard operator framework rather than the vectorized representation.

[4]Here Eq. (A1) is obtained by writing Eq. (24) from [30] as a series, with $S_0 = 1$ the coefficient of the highest-order term in the characteristic polynomial of A.

relation

$$S_m = \frac{d}{2m}\left(1 - \frac{2(m-1)}{d}\right)S_{m-1}. \qquad (A4)$$

With $\delta = 1 + d/2$, this yields

$$S_m > 0 \quad \text{for } 0 \leqslant m < \delta, \qquad (A5)$$

$$S_m = 0 \quad \text{for } \delta \leqslant m \leqslant d, \qquad (A6)$$

which implies that $S_m \geqslant 0 \, \forall \, m$. This result does not depend on k, nor do the coefficients S_m and the roots of the characteristic polynomial, i.e., the eigenvalue of A. Hence, A is positive semidefinite for any choice of $\mathcal{P}_k$ and consequently so is ρ. ∎

---

[1] M. A. Nielsen and I. L. Chuang, *Quantum Computation and Quantum Information*, 10th ed. (Cambridge University Press, Cambridge, 2010).

[2] G. M. D. Ariano, L. Maccone, and M. Paini, Spin tomography, J. Opt. B **5**, 77 (2003).

[3] M. Mohseni, A. T. Rezakhani, and D. A. Lidar, Quantum-process tomography: Resource analysis of different strategies, Phys. Rev. A **77**, 032322 (2008).

[4] I. Bongioanni, L. Sansoni, F. Sciarrino, G. Vallone, and P. Mataloni, Experimental quantum process tomography of non-trace-preserving maps, Phys. Rev. A **82**, 042307 (2010).

[5] I. M. Georgescu, S. Ashhab, and F. Nori, Quantum simulation, Rev. Mod. Phys. **86**, 153 (2014).

[6] K. Temme, S. Bravyi, and J. M. Gambetta, Error Mitigation for Short-Depth Quantum Circuits, Phys. Rev. Lett. **119**, 180509 (2017).

[7] S. Endo, S. C. Benjamin, and Y. Li, Practical Quantum Error Mitigation for Near-Future Applications, Phys. Rev. X **8**, 031027 (2018).

[8] S. Endo, Z. Cai, S. C. Benjamin, and X. Yuan, Hybrid quantum-classical algorithms and quantum error mitigation, J. Phys. Soc. Jpn. **90**, 032001 (2021).

[9] S. Mangini, L. Maccone, and C. Macchiavello, Qubit noise deconvolution, EPJ Quantum Technol. **9**, 29 (2022).

[10] C. Macchiavello and G. M. Palma, Entanglement-enhanced information transmission over a quantum channel with correlated noise, Phys. Rev. A **65**, 050301(R) (2002).

[11] C. Macchiavello, G. M. Palma, and S. Virmani, Transition behavior in the channel capacity of two-qubit channels with memory, Phys. Rev. A **69**, 010303(R) (2004).

[12] C. Macchiavello and M. F. Sacchi, Witnessing quantum capacities of correlated channels, Phys. Rev. A **94**, 052333 (2016).

[13] D. Daems, Entanglement-enhanced transmission of classical information in Pauli channels with memory: Exact solution, Phys. Rev. A **76**, 012310 (2007).

[14] P. Huang, G. He, Y. Lu, and G. Zeng, Quantum capacity of Pauli channels with memory, Phys. Scr. **83**, 015005 (2011).

[15] J. Jiang, K. Wang, and X. Wang, Physical implementability of linear maps and its application in error mitigation, Quantum **5**, 600 (2021).

[16] L. Lautenbacher, F. de Melo, and N. K. Bernardes, Approximating invertible maps by recovery channels: Optimality and an application to non-Markovian dynamics, Phys. Rev. A **105**, 042421 (2022).

[17] A. Gilyén, S. Lloyd, I. Marvian, Y. Quek, and M. M. Wilde, Quantum Algorithm for Petz Recovery Channels and Pretty Good Measurements, Phys. Rev. Lett. **128**, 220502 (2022).

[18] S. T. Flammia and J. J. Wallman, Efficient estimation of Pauli channels, ACM Trans. Quantum Comput. **1**, 1 (2020).

[19] D. Greenbaum, Introduction to quantum gate set tomography, arXiv:1509.02921.

[20] E. Nielsen, J. K. Gamble, K. Rudinger, T. Scholten, K. Young, and R. Blume-Kohout, Gate set tomography, Quantum **5**, 557 (2021).

[21] C. J. Wood, J. D. Biamonte, and D. G. Cory, Tensor networks and graphical calculus for open quantum systems, Quantum Inf. Comput. **15**, 759 (2015).

[22] C. Bény, Quantum deconvolution, Quantum Inf. Process. **17**, 26 (2017).

[23] K. M. R. Audenaert and S. Scheel, On random unitary channels, New J. Phys. **10**, 023011 (2008).

[24] K. Siudzińska, Classical capacity of generalized Pauli channels, J. Phys. A: Math. Theor. **53**, 445301 (2020).

[25] Z. Cai, X. Xu, and S. C. Benjamin, Mitigating coherent noise using Pauli conjugation, npj Quantum Inf. **6**, 17 (2020).

[26] S. Roncallo, L. Maccone, and C. Macchiavello, arXiv:2212.11968

[27] A. D'Arrigo, G. Benenti, G. Falci, and C. Macchiavello, Classical and quantum capacities of a fully correlated amplitude damping channel, Phys. Rev. A **88**, 042337 (2013).

[28] A. D'Arrigo, G. Benenti, G. Falci, and C. Macchiavello, Information transmission over an amplitude damping channel with an arbitrary degree of memory, Phys. Rev. A **92**, 062342 (2015).

[29] M. Hamada, A lower bound on the quantum capacity of channels with correlated errors, J. Math. Phys. **43**, 4382 (2002).

[30] M. S. Byrd and N. Khaneja, Characterization of the positivity of the density matrix in terms of the coherence vector representation, Phys. Rev. A **68**, 062322 (2003).